Microelectronics Reliability 110 (2020) 113650

Contents lists available at ScienceDirect

Microelectronics Reliability

journal homepage: www.elsevier.com/locate/microrel

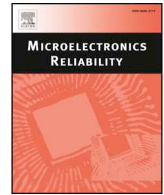

In-situ service load monitoring of automotive electronic systems using silicon-based piezoresistive stress sensor

Yu-Hsiang Yang[a], Bongtae Han[a,*], Alexandru Prisacaru[b], Przemyslaw Gromala[b], Shengbing Jiang[c], Azeem Sarwar[c]

[a] Mechanical Engineering Department, University of Maryland, College Park, MD 20742, USA
[b] Robert Bosch GmbH, Reliability Modeling and System Optimization (AE/EDT3), Reutlingen 72703, Germany
[c] Vehicle Health Management Group, General Motors, Warren, MI 48090, USA

ARTICLE INFO

Keywords:
Piezoresistive stress sensor
In-situ loading
Automotive electronics
Electronic control unit
Multilayer ceramic capacitor
Solder joint

ABSTRACT

It is expected that more and more complex (integrated) automotive electronics will be adopted in systems. These advanced electronics are critical for passenger safety. Documenting the in-situ loading is, thus, very important for accurate reliability prognostics. In this study, we propose a piezoresistive stress sensor to detect the in-situ loading of an automotive electronic control unit (ECU). A load metric directly related to the in-situ loading is defined by considering the in-situ stress values of twelve measurement cells in each sensor. The sensor and the proposed load metric are implemented to document the in-situ loading that results from the local coefficient of thermal expansion mismatch between the electrical components and printed circuit board (PCB) in advanced ECUs. The validity of the proposed metric is corroborated by failure analysis of solder joints of multilayer ceramic capacitors (MLCCs).

1. Introduction

Three major trends in the automotive industry – connectivity, automation and electrification – will continue to accelerate the development of automotive electronics into the future [1]. It is expected that more and more complex (integrated) automotive electronics will appear in the market. Reliability assessment of advanced automotive electronics is extremely critical for passenger safety. The reliability challenge, thus, is one of the critical issues, which must be concerned.

The loading subjected during operation is different from vehicle to vehicle. Various sensors have been used in automobiles to document operating environments such as temperature, vibration, humidity, etc. at [2–4]. It is challenging to infer the stresses of advanced automotive electronics from the conventional sensors due to the complexity of advanced electronics. Adopting more advanced sensors is warranted to document the in-situ loading condition of advanced electronics for accurate reliability prognostics.

The silicon-based piezoresistive stress sensor was developed originally to measure the stresses of a silicon chip embedded in semiconductor packages [5]. More recently, the sensor was implemented successfully in various prognostics and health management (PHM) applications. Roberts et al. found that the stresses during packaging process and thermal cycling testing changed rapidly at the beginning, but had small changes afterward [6–8]. Rahim et al. found that stress sensor signal changed significantly due to delamination and warpage failure [9]. Similar results also were found by Shindler-Saefkow et al. [10] and Yu-Yao Chang et al. [11,12]. Before delamination, Lall et al. observed the changes in stress signal, which can be a possible leading indicator of failure [13,14]. For automotive electronics, various prognostics attempts were performed using the stress sensor. It includes the stress measurement of molded electronic control units and the in-situ failure or fault detection [15–20].

As mentioned earlier, the piezoresistive stress sensor has a unique advantage over conventional sensors; it provides in-situ stresses during operations while conventional sensor provides signals only related to operating conditions. In this study, this advantage is further exploited to propose the stress sensor as an in-situ load counter for advanced automotive electronics. The stress sensor and a proposed load metric are described in Section 2. An implementation of the proposed metric for electronic control units (ECUs) is presented in Section 3 and 4.

2. Load metric of stress sensor signals

The piezoresistive stress sensor is described briefly first. Then, a

* Corresponding author.
E-mail address: bthan@umd.edu (B. Han).

https://doi.org/10.1016/j.microrel.2020.113650
Received 17 October 2019; Received in revised form 14 January 2020; Accepted 6 April 2020
0026-2714/ © 2020 Elsevier Ltd. All rights reserved.

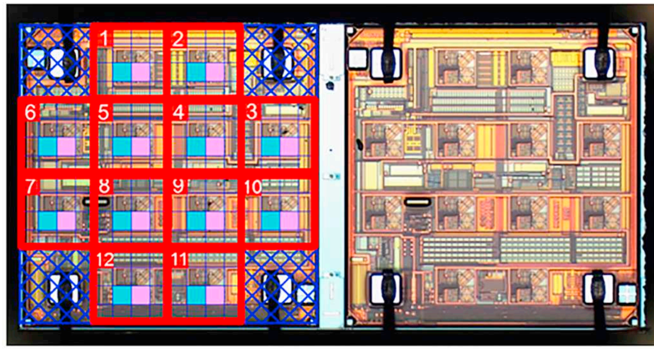

(a)

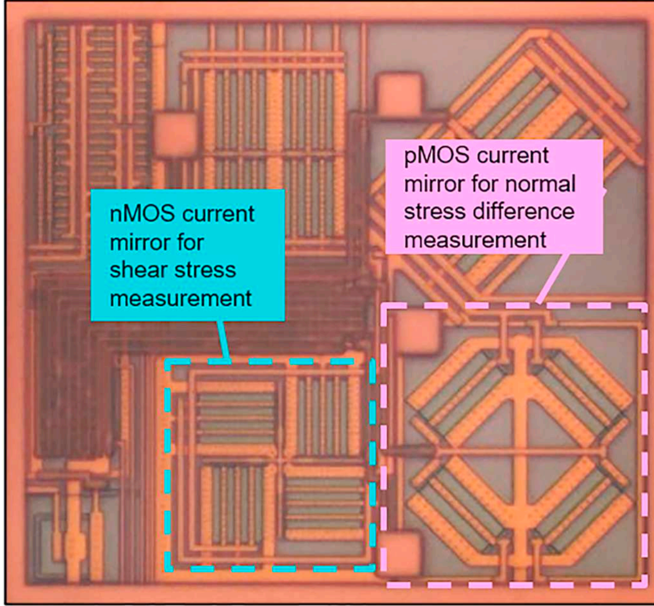

(b)

Fig. 1. (a) Sensor chip containing two sensors where the numbers indicate 12 active measurement cells; and (b) single measurement cell containing two current mirrors in a forward and reverse arrangement for the normal stress difference and shear stress measurements.

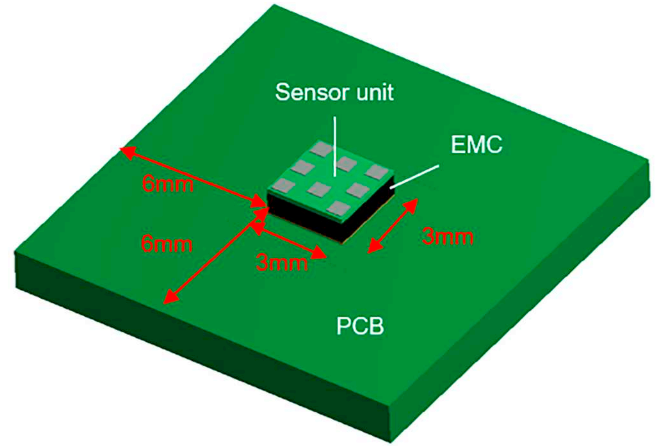

(a)

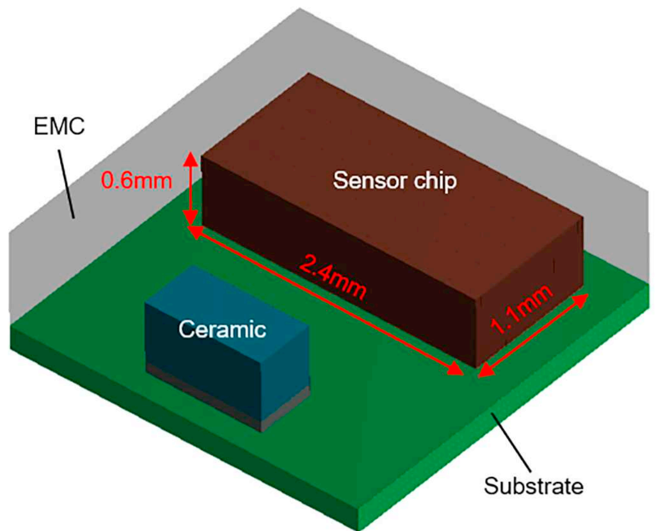

(b)

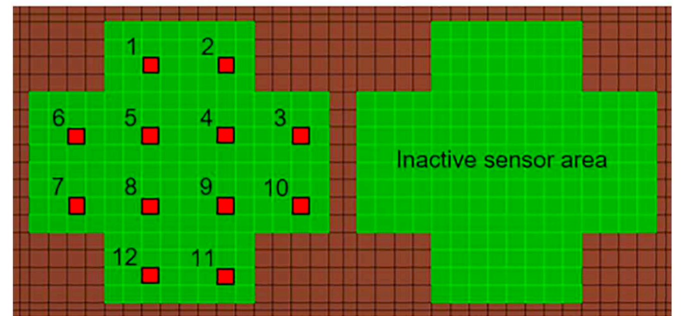

(c)

Fig. 2. Finite-element model used in the stress analysis; (a) a stress sensor unit attached on a PCB using underfill; (b) a sensor chip in a sensor unit; (c) measurement cells of the active stress sensor.

load metric is defined from the results of numerical stress analyses.

2.1. Piezoresistive stress sensor

The sensor used in this paper is a complementary metal-oxide semiconductor (CMOS) piezoresistive stress sensor. The sensing elements consist of channels of metal-oxide-semiconductor field-effect transistors (MOSFETs) in current mirror circuits [5]. When the current mirrors are oriented with respect to the crystallographic axes of silicon ([110] and [100]), the MOSFETs respond differently to the applied mechanical stresses.

The applied stresses obtained from the piezoresistive sensors can be determined from the measured current differences by [5].

$$\sigma_x - \sigma_y = D(\sigma) \approx -\frac{2}{\pi_{44}^{p}(T)}\left(\frac{I_D\,|_{0\circ} - I_D|_{90\circ}}{I_D\,|_{0\circ} + I_D|_{90\circ}}\right) \tag{1}$$

$$\tau_{xy} \approx -\frac{1}{\pi_{D}^{n}(T)}\left(\frac{I_D\,|_{+45\circ} - I_D|_{-45\circ}}{I_D\,|_{+45\circ} + I_D|_{-45\circ}}\right) \tag{2}$$

where σ_x and σ_y are the in-plane normal stress in the x-direction and y-direction, respectively; τ_{xy} is the in-plane shear stress; and are the temperature-dependent piezoresistive coefficients for pMOS and nMOS, respectively, which are influenced by the current mirror circuits; and I_D is the drain current of the current mirrors where the subscripts show the direction of the channels.

The sensor chip is shown in Fig. 1(a). It consists of two sensors, but only one sensor on the left is utilized in this study. Each sensor contains twelve measurement cells placed in a 4 × 4 matrix (red boxes with numbers). The four corner cells are inactive, as they are used as bonding pads. Fig. 1(b) shows one of these twelve identical cells. Each

Table 1
Material properties used in numerical analysis.

Material	Young's modulus (GPa)		CTE (ppm/°C)		Poisson's ratio		T_g (°C)
			Below T_g	Above T_g			
EMC	Temp. dependent		8.2	26.7	0.35 (below T_g)	0.45 (above T_g)	106
Silicon die	170		2.8		0.36		–
Solder (SAC)	Temp. dependent		20		0.36		–
Die attach	Temp. dependent		51	171	Temp. dependent		37.55
Ceramic	107		5		0.25		–
Substrate	22.55		13	15.5	0.35		110
Underfill	6.3 (below T_g)	0.4 (above T_g)	36	120	0.4		137
PCB	22		16		0.28		130

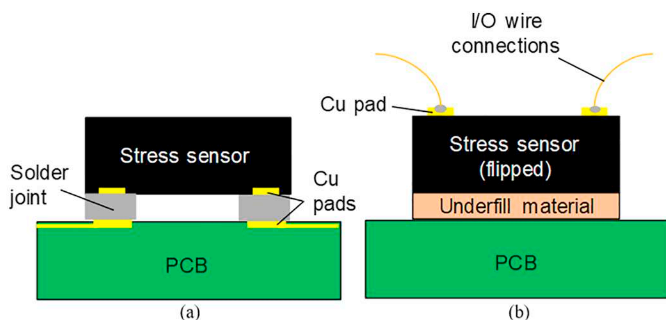

Fig. 3. Stress sensor configurations on the PCB; (a) the sensor is upright and mounted using surface mount technology; and (b) the sensor is flipped upside down and manually attached to the PCB using an epoxy-based underfill.

cell contains two pairs of stress sensitive pMOS and nMOS transistors that independently measure the normal stress differences in Eq. (1) and the shear stress in Eq. (2).

2.2. Load metric

In ECUs, electronic packaging components are typically mounted on the surface of a printed circuit board (PCB). The coefficient of thermal expansion (CTE) mismatch between components and PCB produces the in-plane stresses in interconnections and causes interconnect failures.

The objective of this study aims to count the loading applied to the components. Therefore, a certain load metric, which well represents the effect of CTE mismatch and integrates data from the twelve cells, is required to represent the applied loading.

To understand the stresses distribution on the sensor in different PCB configurations, a finite element analysis (FEA) was conducted. Fig. 2 shows a finite-element model constructed by the commercially available software, ANSYS. Fig. 2(a) and (b) show the dimensions of the sensor unit on a PCB and of the sensor chip, respectively. Fig. 2(c) shows the twelve active sensor cells that are used to represent the measured stresses on the top of sensor chip. Table 1 lists the material properties used in the analysis. This model can predict the stresses in twelve sensing cells induced by CTE mismatch between the sensor and PCB.

The copper pads are exposed on the bottom of the sensor packages, and should have been utilized to mount the package on a PCB using surface mount technology as shown in Fig. 3(a). However, the PCBs used in this study were not designed to accommodate the input/output (I/O) pads of the stress sensors. To cope with the problem, the stress sensors were flipped upside down and manually attached to the PCBs by epoxy-based underfill, as shown in Fig. 3(b). Then, physical wires were soldered to the pads to connect the sensors to the electrical signal and power lines of data acquisition units. Therefore, the FEA model followed the configuration shown in Fig. 3(b).

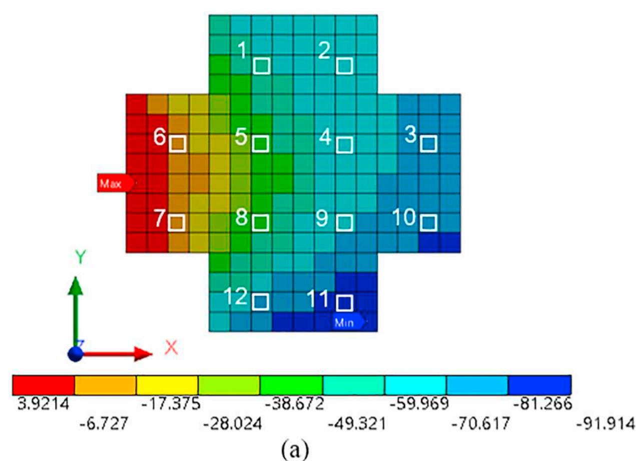

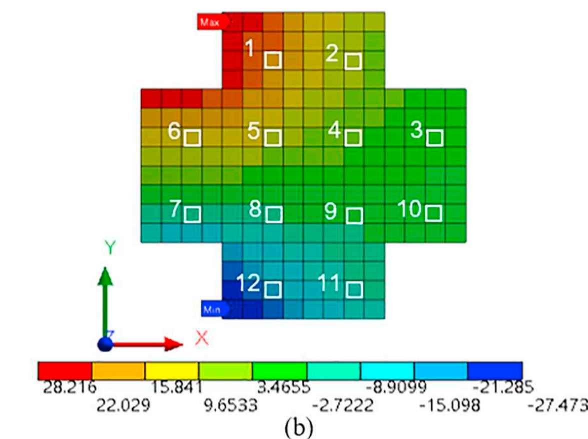

Fig. 4. Distributions of (a) normal stress difference and (b) shear stress on the sensor chip caused by cooling from 150 °C to −55 °C.

Another critical task of the modeling was to produce a detailed representation of the stress sensing cells. The thickness of the MOSFET branch in the actual sensor chip, in which the calculation of the stress was performed, was approximately 10 μm thick. The sensor chip was discretized to produce the 10 μm thick top layer. In addition, each stress-sensing cell was divided into 4 × 4 elements so that the elements matched to the geometry of current mirrors shown in Fig. 1(b). The top view of the mesh is shown in Fig. 2(c) to illustrate the mesh geometry more clearly. The red squares, which closed to the measurement cells showed in Fig. 1(a), are the meshes used to abstract the representative stresses for twelve cells.

The distribution of normal stress difference and shear stress on the sensor chip subjected to a thermal cycle (cooling from 150 °C to

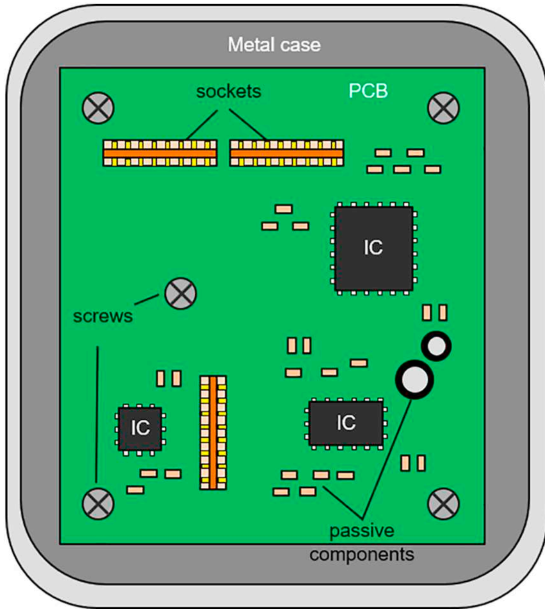

Fig. 5. Schematic illustration of a typical PCB inside an ECU.

−55 °C) is shown in Fig. 4(a) and (b), respectively, assuming that the sensor is stress free at 150 °C. The distribution reveals that the stresses vary between cells due to the non-uniform stress on the sensor chip. A load metric can be defined conceptually using the stress signals from all 12 cells as:

$$\sigma^* \equiv \sum_{i=1}^{12} |(\sigma_x - \sigma_y)^i| \tag{3}$$

or

$$\sigma^* \equiv \sum_{i=1}^{12} |(\tau_{xy})^i| \tag{4}$$

where σ^* is the load metric based on the absolute value of the normal stress difference, $\sigma_x - \sigma_y$, or of the shear stress,τ_{xy}; and i indicates the index of each cell.

A special case arises when two reference points are considered. In this case, a change in the load metric should be used for assessment. Using Eq. (3) or Eq. (4), a change in the load metric can be expressed as:

$$\Delta\sigma^* = \sum_{i=1}^{12} |(\sigma_x - \sigma_y)^i_{T_1} - (\sigma_x - \sigma_y)^i_{T_2}| \tag{5}$$

or

$$\Delta\sigma^* = \sum_{i=1}^{12} |(\tau_{xy})^i_{T_1} - (\tau_{xy})^i_{T_2}| \tag{6}$$

where T_1 and T_2 are two reference temperatures, and $\Delta\sigma^*$ is a change in the load metric between two reference temperatures.

As illustrated in Fig. 5 schematically, an ECU containing a PCB screwed into a metal enclosure. There are many components, such as active integrated circuits (IC) devices, capacitors, resistors, and sockets etc., mounted on the PCB. The architectural design (i.e., the location of the screws and components on the PCB) will affect the local deformation and thus the local CTE of the PCB. The local CTE of the PCB near the screws is larger than the global CTE far from the screws because the metal case, which has a larger CTE than the PCB, forces the PCB to deform more. Similarly, the location of the PCB with high density of components has a different CTE than the location of PCB with no components.

Simulations under various CTEs of PCBs were performed to investigate the effectiveness of the load metric; i.e., how effectively the load metric established in Eqs. (5) and (6) can represent the thermally-induced stress levels. In the simulation, the load metrics were calculated with varying PCB CTEs (10 ppm to 24 ppm). The range of the CTE was chosen considering the CTE of typical aluminum enclosure and the CTE of electrical components. Detailed normal stress difference and shear stress of each cell for three representative CTE values of PCB are shown in Fig. 6 (a) and (b), respectively. The normal stress difference of each cell increases with the CTE except for Cells 6 and 7 where the magnitudes of σ_x and σ_y are virtually the same. On the other hand, the distribution of τ_{xy} does not change significantly, as the CTE mismatch affects τ_{zy} or τ_{zx}.

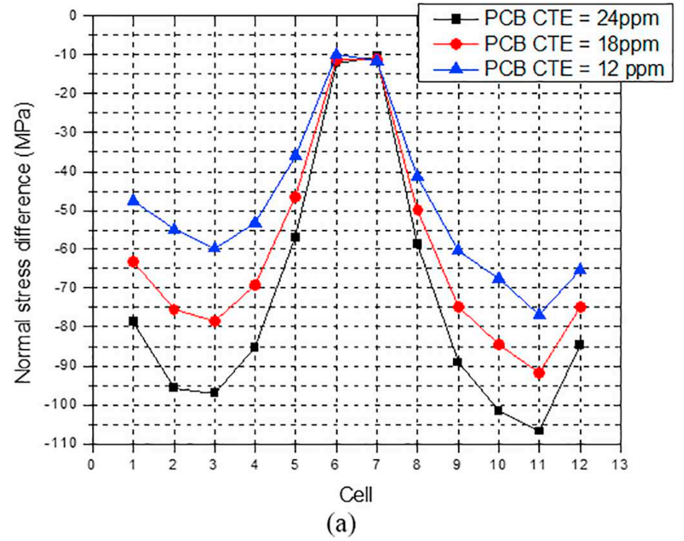

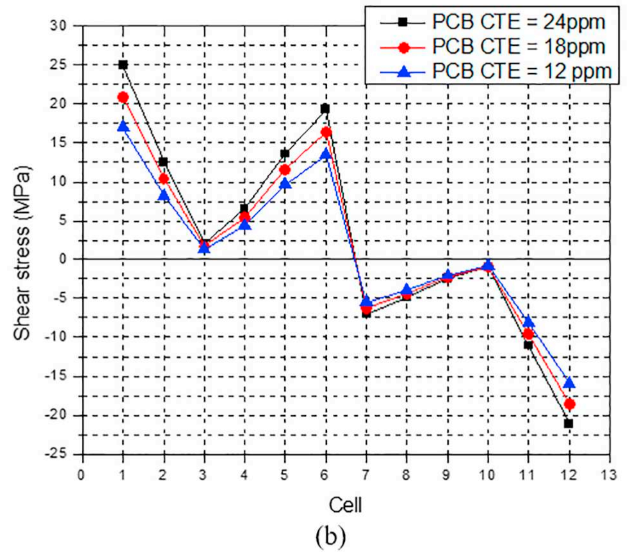

Fig. 6. (a) Normal stress difference and (b) shear stress from twelve cells with three different CTEs of PCB (12 ppm, 18 ppm and 24 ppm), caused by cooling from 150 °C to −55 °C.

The load metrics vs. the CTE of PCB is shown in Fig. 7. It clearly portrays the linear relationship between load metric and CTE. As expected, the in-plane normal stress difference is much more sensitive to the CTE mismatch than the shear stress. For this reason, the load metric based on normal stress difference will be used for the following analysis. In addition, the normal stress difference of each cell changes consistently, as the CTE of PCB increases. This result provides an additional technical rationale for the load metric; i.e., that the summation of absolute normal stress differences represents effectively the effect of

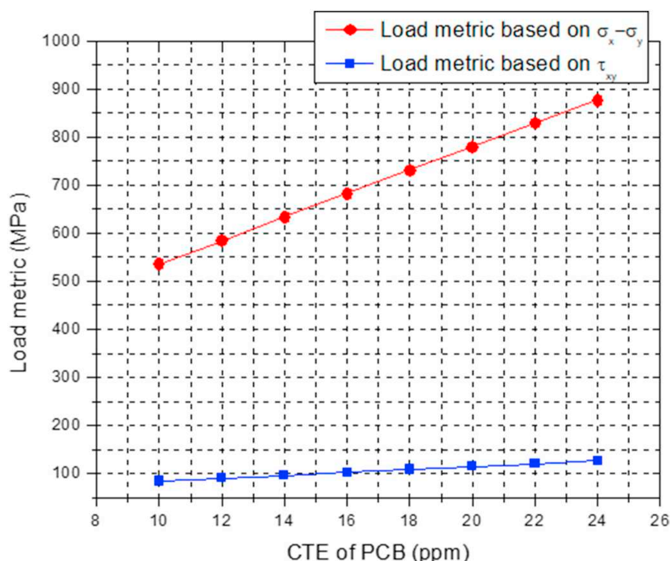

Fig. 7. Load metrics determined from twelve cells with CTEs of PCB vary from 10 ppm to 24 ppm subjected to temperature cooling from 150 °C to −55 °C; the blue and red lines indicate the load metrics based on the shear stress and the normal stress difference, respectively. (For interpretation of the references to color in this figure legend, the reader is referred to the web version of this article.)

the load metric caused by thermally-induced stress. This process also eliminates uncertainties associated with the inherent signal noise of the sensor [5].

3. Test and results

The piezoresistive stress sensors are used to measure the stress loading (load metric) on the different locations of PCBs inside the test vehicle ECUs. Then, the test vehicles were subjected to long-term thermal cycling to verify the relationship between the load metric and the actual damage level of solder interconnects.

3.1. Test vehicle and stress sensor placements

Two identical ECUs, ECU-1 and ECU-2, were used in this study. Fig. 8 shows the ECU, which is utilized in an advanced cruise system. As shown in Fig. 8(a), the dimensions of each ECU are ≈19 cm × 19 cm × 5 cm, and each ECU is composed of two halves. Each half includes a PCB. Fig. 8(b)–(e) show the top and bottom of each PCB. The PCBs are fixed to an aluminum case by five screws (blue circles in the Fig. 8(b)–(e)). Many components are mounted on both sides of PCBs, such as IC devices, capacitors, resistors and sockets (red rectangles).

It is important to note that these components and screws were not distributed uniformly on the PCBs. Eight stress sensors were placed at various locations to document the effect of local constraints (e.g., fixed screws and sockets). The sensor locations are shown schematically in Fig. 8(a), where "T" and "B" denote the top and bottom PCB, respectively. Table 2 lists the characteristics of eight sensor locations in the test vehicle, which are shown as yellow rectangles in Fig. 8(a)–(e).

3.2. Loading conditions and measurements

The two ECUs were tested inside a thermal cycling chamber (GB-16-5-5-WC; Russells). The minimum and maximum temperatures were −55 °C and 150 °C, respectively. Fig. 9 shows the actual temperature profile used in the test. The temperature was held constant at −55 °C and 150 °C for 20 min each, and was increased or decreased between

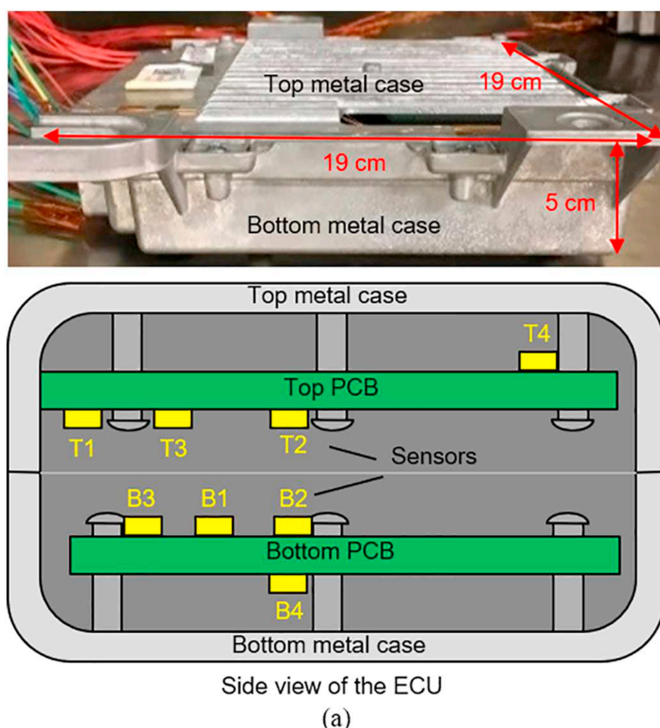

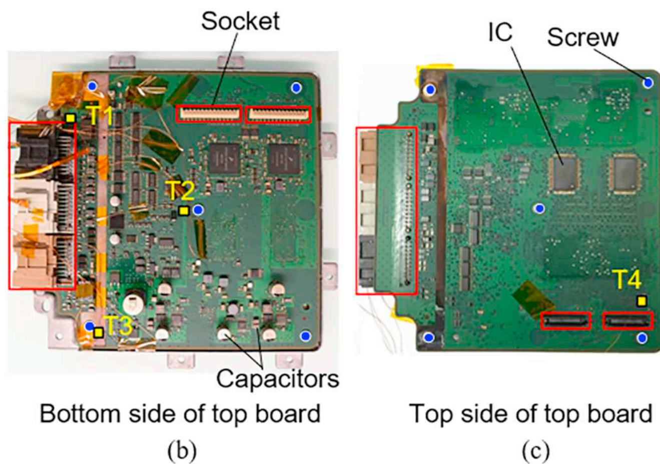

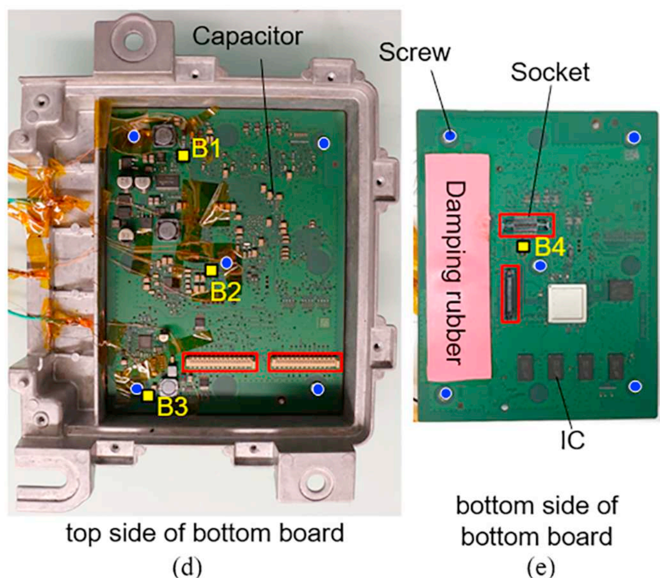

(caption on next page)

Fig. 8. Configuration of ECU test vehicle: (a) side view; (b) and (c) are the bottom view and top view of top half, respectively; (d) and (e) are the top view and bottom view of bottom half, respectively. Blue circles, red rectangles and yellow rectangles indicate screws, sockets and stress sensor placements, respectively. (For interpretation of the references to color in this figure legend, the reader is referred to the web version of this article.)

Table 2
Characteristics of sensor locations.

Sensor location	B1	B2	B3	B4	T1	T2	T3	T4
Distance to the closest constraints:								
Screw	21	3.8	2.0	3.0	20	3.0	4.2	11.0
Component	< 2.0	1.8	< 1.0	4.9	3.7	4.2	4.0	< 1.0
Socket	> 30	> 30	20	4.9	4.8	> 30	28.0	< 1.0

Unit: mm

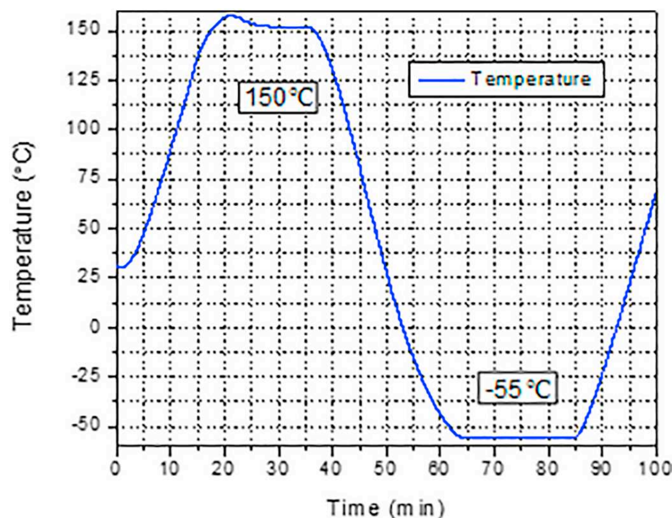

Fig. 9. Temperature profile of the thermal cycling test.

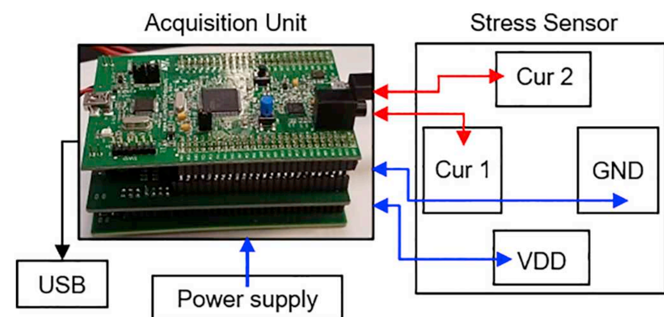

Fig. 10. Data acquisition unit and its electrical connection.

the two extremes with a ramp rate 10 °C/min. Each cycle took around 95 min.

The data from the sensors was collected by a dedicated acquisition unit (Fig. 10). Control over the whole process was taken by a microcontroller. All inputs of the sensors were controlled by a digital-to-analog converter (DAC). It includes a voltage generator, which supplies power to the chip as well as the current source. Both of them were designed to ensure good stability and accuracy.

Outputs from the chip were digitalized by an analog-to-digital converter (ADC). The acquisition unit was able to measure eight sensors simultaneously. Each ECU contained eight stress sensors, and one independent acquisition unit was designated to each ECU to collect the

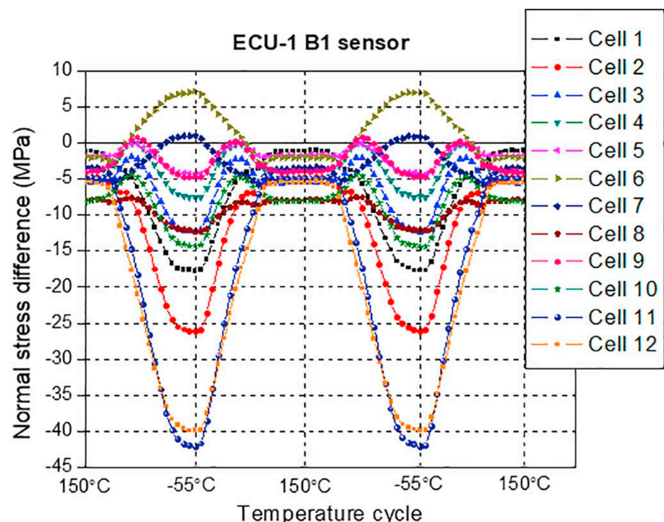

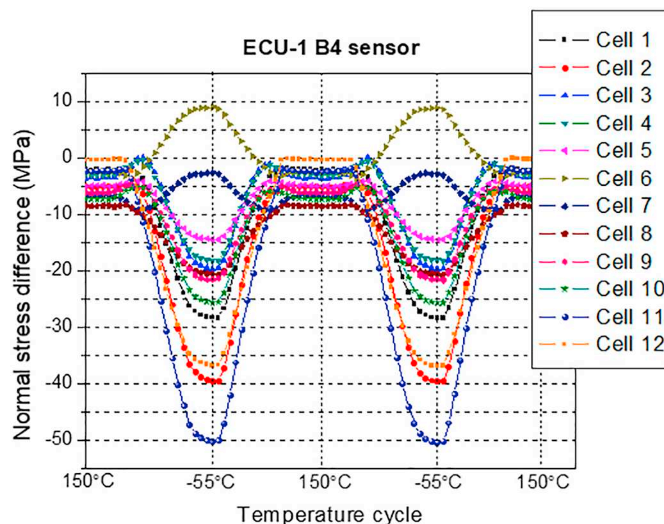

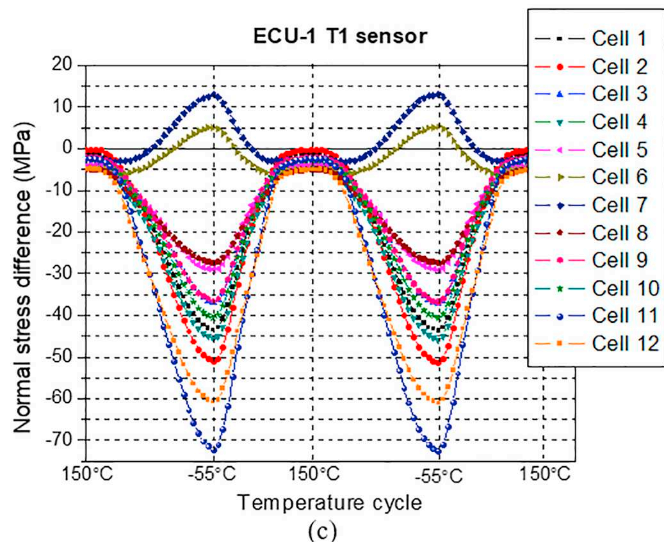

Fig. 11. Normal stress difference of (a) a B1 sensor, (b) a B4 sensor and (c) a T1 sensor in ECU-1 measured during two temperature cycles.

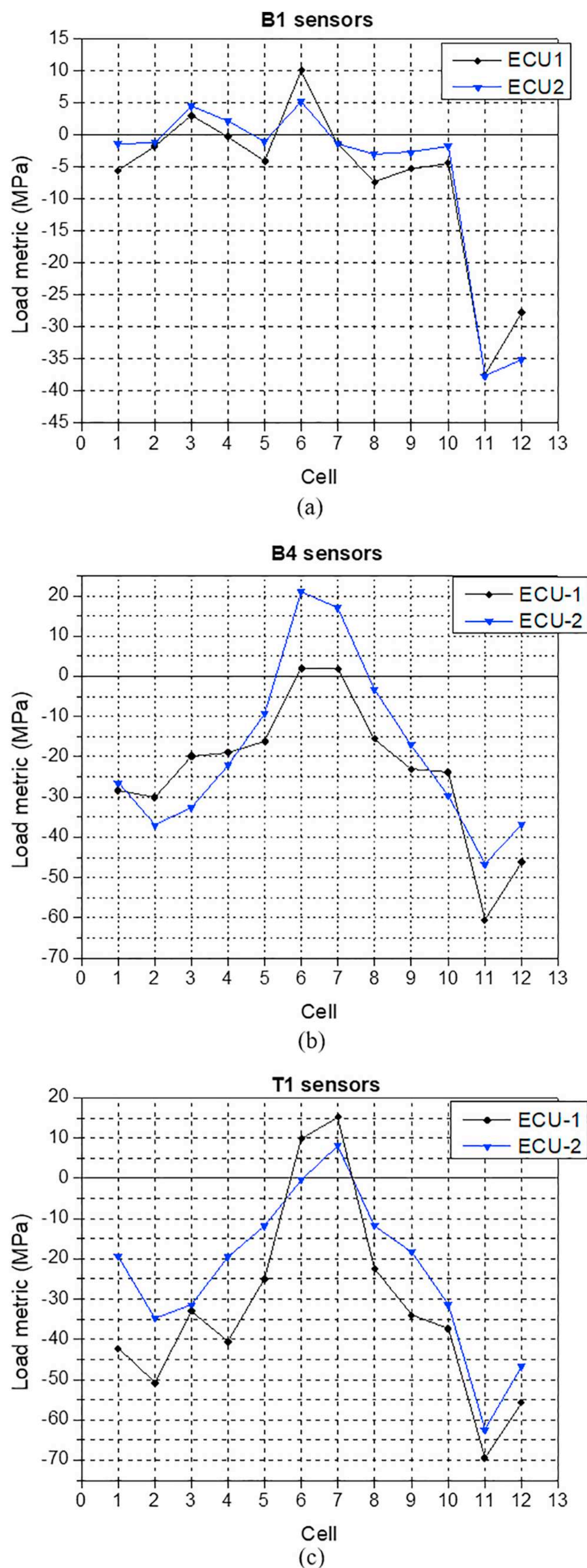

Fig. 12. Load metric components of two ECUs, defined by Eq. (5), where are −55 °C and 150 °C: (a) B1 sensors, (b) B4 sensors and (c) T1 sensors.

stress data under the thermal loadings. Fig. 10 also illustrates the electrical connections of acquisition unit. The blue and red lines transfer power and signal, respectively. CUR 1 and 2 were used to measure the current differences in current mirror circuits mentioned in section 2. VDD and GND were used for connecting positive supply voltage and ground, respectively.

3.3. Load metric results

Fig. 11(a)–(c) shows representative normal stress differences measured from three sensors, B1, B4 and T1, in ECU-1 during two temperature cycles. It clearly shows that the stresses were changed with temperature caused by CTE mismatch, and the changes in the stresses vary between cells which compatible with the simulation result. The most of normal stress differences at 150 °C are significantly smaller than the one measured at −55 °C. This is because the modulus of the EMC used for the sensor unit decreased as the test temperature increased.

The change in the load metric over the temperature cycle was obtained by using Eq. (5), where T_1 and T_2 were150 °C and −55 °C, respectively. Fig. 12(a)–(c) plots examples of the load metrics of three sensors, B1, B4 and T1, in both ECU-1 and ECU-2. It shows a similar load metric from ECU to ECU but significantly different load metric from sensor to sensor.

Fig. 13 plots the load metric value of each sensor from both ECUs. The load metric values range from 97 MPa to 436 MPa, clearly indicating that the load metric values are highly location-dependent.

The plot also shows large variations of the load metric in several sensors, i.e. T1 and T2, between both ECUs. It is speculated that the thickness of manually dispensed adhesive is attributed to the load metric variations.

3.4. Effect of load metric

The solder joint crack is one of the most common failures in electronic devices. It is one of the major failure modes caused by CTE mismatch between the PCB and electrical components. Once small cracks in solder joint are formed, they will propagate and may cause open circuit failures. It is important to recall that the proposed load metric is sensitive to the local CTE of the PCB. Thus, it is expected that the load metric value would represent the damage of solder joints.

After obtaining the load metric, the ECUs were continuously subjected to the thermal loading for 1000 cycles. Failure analyses of solder joints between multilayer ceramic capacitors (MLCCs) and PCBs were followed to validate the relationship between the levels of load metrics and reliability of electrical components. Based on the availability of identical MLCCs near the sensors, the MLCCs which were close to the sensors T1, T2, and B1 were selected for failure analyses. It is to be noted that the values of load metric measured from T1, T2 and B1 represent the high (≥325 MPa), mid (≃250 MPa), and low (≃100 MPa) load metric values, respectively.

Fig. 14 shows the cross-sectional view of the selected type of MLCC used in failure analyses. Fig. 15 shows the cross-sections of solder joints between PCB and MLCCs, which have the high, mid and low load metrics from both of ECU units. The MLCCs near sensors that have high load metrics have severe damage to the solder joint. On the other hand, the MLCCs near sensors that have low load metrics have less damage to the solder joint. The results clearly indicate that the load metric represents the local loading conditions accurately.

4. Conclusions

A piezoresistive stress sensor was proposed to detect the in-situ loading of an automotive electronic control unit (ECU) to cope with the limitations of conventional sensors that provide signals only related to operating conditions. The sensor was implemented successfully to document different levels of loadings inside the advanced ECUs. The

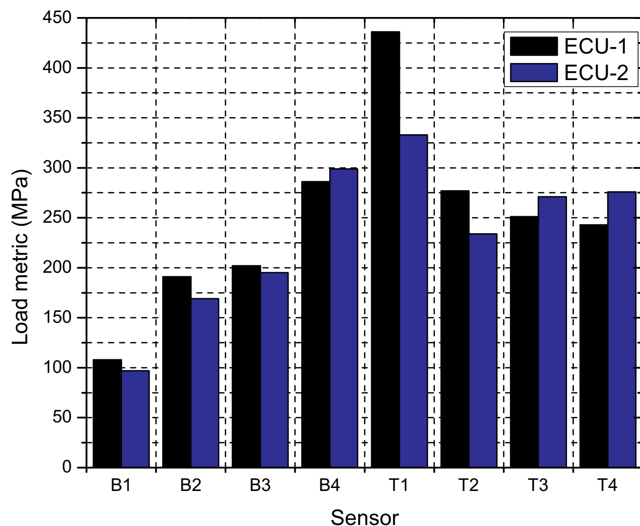

Fig. 13. Load metric values of each sensor.

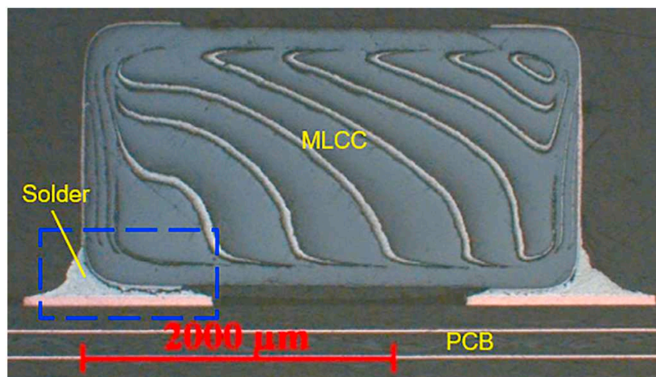

Fig. 14. Cross-sectional view of the selected multilayer ceramic capacitor.

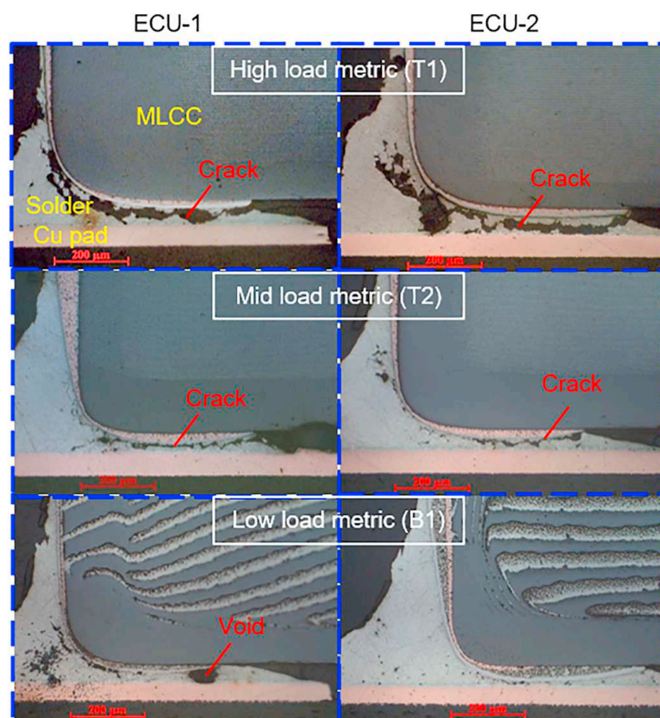

Fig. 15. Cross-sectional views of the solder joints of MLCCs, placed near the sensors that have high, mid and low load metric values.

failure analyses of solder joints between multilayer ceramic capacitors (MLCCs) and printed circuit boards (PCBs) were followed after subjecting ECUs to 1000 thermal cycles. The results showed a clear correlation between the damage levels of MLCCs' solder joints and load metric rankings, which corroborated the validity of the proposed method.

The proposed approach can be extended to actual vehicles driven in very different environments. In-situ loading conditions measured from the stress sensor, then, can be used for health management of critical ECUs in the vehicles. It is anticipated for the near future that the stress sensor will be eventually embedded in actual power semiconductor devices such as insulated-gate bipolar transistors for health management of active devices.

Credit authorship contribution statement

Yu-Hsiang Yang: Methodology, Validation, Formal analysis, Investigation, Data curation, Writing - original draft, Visualization, Supervision. **Bongtae Han:** Conceptualization, Methodology, Validation, Formal analysis, Investigation, Data curation, Writing - original draft, Writing - review & editing, Visualization, Supervision, Project administration. **Alexandru Prisacaru:** Conceptualization, Methodology. **Przemyslaw Gromala:** Conceptualization, Methodology, Validation, Investigation, Resources, Writing - review & editing, Supervision, Project administration, Funding acquisition. **Shengbing Jiang:** Conceptualization, Validation, Resources, Writing - review & editing, Supervision, Project administration, Funding acquisition. **Azeem Sarwar:** Conceptualization, Resources, Funding acquisition.

Declaration of competing interest

We declare that we have no financial and personal relationships with other people or organizations that can inappropriately influence our work, there is no professional or other personal interest of any nature or kind in any product.

Acknowledgement

This work was supported by the Center for Advanced Life Cycle Engineering (CALCE) of the University of Maryland. Their support is greatly appreciated and graciously acknowledged.

References

[1] P.J. Gromala, A. Prisacaru, M. Jeronimo, H.-S. Lee, Y. Sun, B. Han, Non-linear viscoelastic modeling of epoxy based molding compound for large deformations encountered in power modules, Electronic Components and Technology Conference (ECTC), 2017 IEEE 67th, IEEE, 2017, pp. 834–840.
[2] W.J. Fleming, New automotive sensors—a review, IEEE Sensors J. 8 (11) (2008) 1900–1921.
[3] D.A. Dekate, Prognostics and engine health management of vehicle using automotive sensor systems, Int. J. Sci. Res 2 (2) (2013) 244–251.
[4] A. Ismail, W. Jung, Recent Development of Automotive Prognostics, Korean Reliability Society, 2015, pp. 147–153.
[5] A. Prisacaru, A. Palczynska, P. Gromala, B. Wu, B. Han, G.Q. Zhang, Accuracy of CMOS-Based piezoresistive stress sensor for engineering applications of thermal loading condition: theoretical review and experimental validation, IEEE Sensors J. 19 (20) (2019) 9139–9148.
[6] J. Roberts, et al., Characterization of microprocessor chip stress distributions during component packaging and thermal cycling, 2010 Proceedings 60th Electronic Components and Technology Conference (ECTC), IEEE, 2010, pp. 1281–1295.
[7] J. Roberts, M. Motalab, S. Hussain, J.C. Suhling, R.C. Jaeger, P. Lall, Measurement of die stresses in microprocessor packaging due to thermal and power cycling, 2012 IEEE 62nd Electronic Components and Technology Conference, IEEE, 2012, pp. 756–770.
[8] J.C. Roberts, M.K. Rahim, S. Hussain, J.C. Suhling, R.C. Jaeger, P. Lall, Die stress variation in area array components subjected to accelerated life testing, 2008 11th Intersociety Conference on Thermal and Thermomechanical Phenomena in Electronic Systems, IEEE, 2008, pp. 705–713.
[9] M.K. Rahim, J. Roberts, J.C. Suhling, R.C. Jaeger, P. Lall, Continuous in-situ die stress measurements during thermal cycling accelerated life testing, 2007 Proceedings 57th Electronic Components and Technology Conference, IEEE, 2007, pp. 1478–1489.
[10] F. Schindler-Saefkow, et al., Stress chip measurements of the internal package stress for

process characterization and health monitoring, 2012 13th International Thermal, Mechanical and Multi-Physics Simulation and Experiments in Microelectronics and Microsystems, IEEE, 2012, pp. 1/10–10/10.

[11] Y.-Y. Chang, H. Chung, B.-J. Lwo, R.-T. Tan, K.-F. Tseng, In-situ reliability monitoring on PBGA packaging through piezoresistive stress sensor, 2010 5th International Microsystems Packaging Assembly and Circuits Technology Conference, IEEE, 2010, pp. 1–4.

[12] Y.-Y. Chang, H. Chung, B.-J. Lwo, K.-F. Tseng, In situ stress and reliability monitoring on plastic packaging through piezoresistive stress sensor, IEEE Trans. Compon. Packag. Manuf. Technol. 3 (8) (2013) 1358–1363.

[13] P. Lall, M.N. Islam, M.K. Rahim, J.C. Suhling, Prognostics and health management of electronic packaging, IEEE Trans. Comp. Pack. Technol. 29 (3) (2006) 666–677.

[14] P. Lall, N. Islam, K. Rahim, J. Suhling, S. Gale, Leading indicators-of-failure for prognosis of electronic and MEMS packaging, 2004 Proceedings. 54th Electronic Components and Technology Conference (IEEE Cat. No. 04CH37546), vol. 2, IEEE, 2004, pp. 1570–1578.

[15] P. Gromala, et al., Internal stress state measurements of the large molded electronic control units, 2013 14th International Conference on Thermal, Mechanical and Multi-Physics Simulation and Experiments in Microelectronics and Microsystems (EuroSimE), IEEE, 2013, pp. 1–8.

[16] P. Gromala, A. Palczynska, B. Han, Prognostic approaches for the wirebond failure prediction in power semiconductors: a case study using DPAK package, 2015 16th International Conference on Electronic Packaging Technology (ICEPT), IEEE, 2015, pp. 413–418.

[17] A. Palczynska, P.J. Gromala, D. Mayer, B. Han, T. Melz, In-situ investigation of EMC relaxation behavior using piezoresistive stress sensor, 2015 16th International Conference on Thermal, Mechanical and Multi-Physics Simulation and Experiments in Microelectronics and Microsystems, IEEE, 2015, pp. 1–5.

[18] A. Palczynska, A. Prisacaru, P.J. Gromala, B. Han, D. Mayer, T. Melz, Towards prognostics and health monitoring: the potential of fault detection by piezoresistive silicon stress sensor, Microelectron. Reliab. 74 (2017) 165–172.

[19] A. Prisacaru, A. Palczynska, A. Theissler, P. Gromala, B. Han, G.Q. Zhang, In situ failure detection of electronic control units using piezoresistive stress sensor, IEEE Trans. Compon. Packag. Manuf. Technol. 8 (5) (2018) 750–763.

[20] B. Wu, D.-S. Kim, B. Han, A. Palczynska, A. Prisacaru, P.J. Gromala, Hybrid approach to conduct failure prognostics of automotive electronic control unit using stress sensor as in situ load counter, IEEE Trans. Compon. Packag. Manuf. Technol. 99 (2018) 1–11.